Published in
Journal of Applied Physics 104, issue 9, 093501 1-8, 2008
which should be used for any reference to this work

GaN/AlN short-period superlattices for intersubband optoelectronics: A systematic study of their epitaxial growth, design, and performance

P. K. Kandaswamy,[1] F. Guillot,[1] E. Bellet-Amalric,[1] E. Monroy,[1,a)] L. Nevou,[2] M. Tchernycheva,[2] A. Michon,[2] F. H. Julien,[2] E. Baumann,[3] F. R. Giorgetta,[3] D. Hofstetter,[3] T. Remmele,[4] M. Albrecht,[4] S. Birner,[5] and Le Si Dang[6]

[1] *Equipe Mixte CEA-CNRS Nanophysique et Semiconducteurs, INAC/SP2M/PSC, CEA-Grenoble, 17 rue des Martyrs, 38054 Grenoble Cedex 9, France*
[2] *Action OptoGaN, Institut d'Electronique Fondamentale (CNRS UMR 8622), Université Paris-Sud, 91405 Orsay Cedex, France*
[3] *Institute of Physics, University of Neuchatel, 1 A.-L. Breguet, CH-2000 Neuchatel, Switzerland*
[4] *Institut für Kristallzüchtung, Max-Born-Strasse 2, D-12489 Berlin, Germany*
[5] *Walter Schottky Institute and Physics Department, Technische Universität München, Am Coulombwall 3, D-85748 Garching, Germany*
[6] *Equipe Mixte CEA-CNRS Nanophysique et Semiconducteurs, Institut Néel, CNRS Département Nano, 25 Avenue des Martyrs, 38042 Grenoble Cedex 9, France*

We have studied the effect of growth and design parameters on the performance of Si-doped GaN/AlN multiquantum-well (MQW) structures for intersubband optoelectronics in the near infrared. The samples under study display infrared absorption in the 1.3–1.9 μm wavelength range, originating from the photoexcitation of electrons from the first to the second electronic level in the QWs. A commonly observed feature is the presence of multiple peaks in both intersubband absorption and interband emission spectra, which are attributed to monolayer thickness fluctuations in the quantum wells. These thickness fluctuations are induced by dislocations and eventually by cracks or metal accumulation during growth. The best optical performance is attained in samples synthesized with a moderate Ga excess during the growth of both the GaN QWs and the AlN barriers without growth interruptions. The optical properties are degraded at high growth temperatures (>720 °C) due to the thermal activation of the AlN etching of GaN. From the point of view of strain, GaN/AlN MQWs evolve rapidly to an equilibrium average lattice parameter, which is independent of the substrate. As a result, we do not observe any significant effect of the underlayers on the optical performance of the MQW structure. The average lattice parameter is different from the expected value from elastic energy minimization, which points out the presence of periodic misfit dislocations in the structure. The structural quality of the samples is independent of Si doping up to 10^{20} cm^{-3}. By contrast, the intersubband absorption spectrum broadens and blueshifts with doping as a result of electron-electron interactions. This behavior is independent of the Si doping location in the structure, either in the QWs or in the barriers. It is found that the magnitude of the intersubband absorption is not directly determined by the Si concentration in the wells. Instead, depending on the Al mole fraction of the cap layer, the internal electric field due to piezoelectric and spontaneous polarization can deplete or induce charge accumulation in the QWs. In fact, this polarization-induced doping can result in a significant and even dominant contribution to the infrared absorption in GaN/AlN MQW structures.

I. INTRODUCTION

Intersubband (ISB) transitions in semiconductor quantum wells (QWs) have proven their capability for optoelectronics in the mid- and far-infrared spectral regions. ISB photodetectors present advantages in comparison with interband devices in terms of speed and reproducibility. Furthermore, ISB quantum cascade (QC) lasers are a new and rapidly evolving technology with advantages such as their intrinsic wavelength tailorability, high-speed modulation capabilities, large output powers, operation above room temperature, and fascinating design potential. These features make them particularly promising for applications in terabit optical data communications or ultraprecision metrology and spectroscopy. The potential of QC lasers as trace gas sensors for environmental, automotive, or medical applications have already been proved in the mid- or far-infrared spectral range, using semiconductor materials such as GaAs/AlGaAs, InGaAs/AlInAs-on-InP or InAs/AlSb.

The extension of ISB optoelectronics toward the near infrared spectral region is interesting for the development of ultrafast photonic devices for optical telecommunication networks, as well as for application in a variety of chemical and biological sensors (pollution detection, chemical forensics, chemical and biological warfare, industrial process monitor-

[a)]Author to whom correspondence should be addressed. Electronic mail: eva.monroy@cea.fr.

ing, and medical diagnostics). Material systems with large enough conduction band offset to accommodate ISB transitions at these relatively short wavelengths include InGaAs/AlAsSb,[1] (CdS/ZnSe)/BeTe,[2] GaInNAs/AlAs,[3] and GaN/Al(Ga,In)N QWs.[4–11] In the case of III-nitride heterostructures, their conduction-band offset—around 1.8 eV for the GaN/AlN system—[7,10,12–14] is large enough to develop ISB devices operating in the fiber-optics transmission windows at 1.3 and 1.55 μm. A specific advantage of III nitrides is their extremely short ISB absorption recovery times [$\sim$140–400 fs (Refs. 15–20)] due to the strong electron-phonon interaction in these materials, which opens the way for devices operating in the 0.1–1 Tbit/s bit-rate regime. Furthermore, the remote lateral valleys lie very high in energy ($>$2 eV above the Γ valley[21,22]), which is a key feature to achieve ISB lasing. Finally, devices would benefit from other advantages of the nitride technology, such as high power handling capabilities and chemical and thermal robustness.

In the last few years, various groups have reported ISB absorption at 1.3–1.55 μm in GaN/Al(Ga)N nanostructures in the form of QWs (Refs. 4–10, 17, and 23) or quantum dots.[24–26] The first GaN/AlN photovoltaic QW infrared photodetectors (QWIP),[27–32] lateral transport quantum dot infrared photodetectors,[33,34] and QC detectors[35] have been recently demonstrated. Additionally, there has been an important research effort on saturable absorbers for ultrafast all-optical switching.[19,36–38] GaN-based all-optical switches with an extinction ratio larger than 10 dB have been demonstrated.[37,38]

Strong electronic coupling in double GaN/AlN QWs has been reported,[39,40] which sets the basis for the fabrication of ISB modulators and unipolar lasers. The first demonstrations of electromodulated absorption at 1.3–1.55 μm based on ISB transitions in III-nitride nanostructures have been recently reported.[41–43] Finally, room-temperature ISB photoluminescence from GaN/AlN QWs and quantum dots at wavelengths down to $\lambda=1.5$ μm has been observed at room temperature.[44,45] Despite several theoretical proposals,[46–51] lasing action has not been achieved so far.

Further progress in this field requires a precise control of the epitaxial growth of GaN/AlN multiquantum-well (MQW) structures, paying particular attention to the effects of Si doping and strain distribution. Furthermore, due to the lattice mismatch in the GaN/AlN system and the giant internal electric fields in nitride heterostructures, the presence of the cladding layers can result in polarization-induced doping or depletion of the active superlattice. Thus, the device design must address the structure as a whole and not only the active region.

In this work, we present a systematic investigation on the epitaxial growth, structural, and optical properties of Si-doped GaN/AlN short-period superlattices for ISB applications in the telecommunication spectral range. We first compare different growth procedures using Ga excess during the growth of both GaN and AlN, using In as a surfactant or using Ga excess during GaN growth, and Al excess during the growth of the AlN barriers. Then, we discuss the optical properties of optimized structures. Finally the effects of parameters such as growth temperature, choice of substrate, or silicon doping on the structural properties and optical performance of the structures are presented. Results are interpreted by comparison with theoretical calculations of the electronic structure using a self-consistent 8-band-$\mathbf{k}\cdot\mathbf{p}$ Schrödinger–Poisson solver.

II. EXPERIMENTAL METHODS

Samples are grown by plasma-assisted molecular-beam epitaxy (PAMBE) in a MECA2000 chamber equipped with standard effusion cells for Ga, Al, In, and Si, and a radio-frequency plasma cell to provide active nitrogen. Substrates consist of a 1-μm-thick AlN layer deposited on c-sapphire by metalorganic vapor phase epitaxy (MOVPE). The PAMBE growth rate was fixed at 0.3 ML/s ($\sim$270 nm/h).

The structural properties of the MQWs have been analyzed by high-resolution x-ray diffraction (HRXRD) measurements using a SEIFERT XRD 3003 PTS-HR diffractometer with a beam concentrator prior to the Ge(220) four-bounce monochromator and a Ge(220) two-bounce analyzer in front of the detector. In the case of samples containing AlGaN ternary alloys, the Al mole fraction was calibrated by measuring 1-μm-thick AlGaN layers deposited under the same growth conditions using energy dispersive x-ray spectroscopy in a JEOL JSM-840A scanning electron microscope. The surface morphology of the MQW structures was analyzed by atomic force microscopy (AFM) in the tapping mode, using a Dimension 3100 system.

Photoluminescence (PL) was excited with the 244 nm line of a frequency-doubled continuous-wave Ar^{++} laser and analyzed by a 0.46 m focal length spectrometer equipped with a charge-coupled device (CCD) camera. Cathodoluminescence (CL) experiments were performed in FEI Quanta200 scanning electron microscope equipped with a Jobin Yvon HR460 monochromator and a CCD camera. For infrared absorption measurements, samples were mechanically polished to form a 45° multipass waveguide with 4–5 total internal reflections. The infrared transmission for TM- and TE-polarized light was measured at room temperature using a Fourier transform infrared (FTIR) spectrometer and either a deuterated triglycine sulfate or a mercury-cadmium telluride photodetector.

III. RESULTS AND DISCUSSION

A. Growth and structural characterization

The growth of GaN(0001) by PAMBE is extensively discussed in the literature,[52–56] and it requires a precise control of the metal-to-nitrogen (III/V) flux ratio. GaN deposition under N-rich conditions results in facetted layers with a high surface roughness. Deposition of two-dimensional (2D) GaN layers requires Ga-rich conditions, and hence growth optimization translates into the determination of the adequate metal excess and growth temperature. At a substrate temperature higher than 700 °C and for a certain range of Ga fluxes corresponding to slightly Ga-rich conditions, the Ga excess remains on the growing surface in a situation of dynamical equilibrium, i.e., the Ga coverage is independent of the Ga exposure time. It is possible to stabilize a Ga amount from below 1 up to 2.5 ML. However, smooth surfaces can only

be achieved with a Ga coverage of 2.5 ± 0.1 ML,[52,53] when the Ga excess arranges into a so-called "laterally contracted Ga bilayer,"[56–58] which consists of two Ga layers adsorbed on top of the Ga-terminated (0001) GaN surface. The first Ga adlayer is supposed to be pseudomorphic to the GaN surface, but the second Ga adlayer is laterally contracted, presenting an in-plane lattice constant close to the Ga–Ga bond length in bulk Ga ($\sim$2.75 Å). For higher Ga fluxes, the Ga coverage depends on the exposure time, indicating a droplet accumulation regime.

An alternative to metal rich conditions is the use of a surfactant to enhance 2D growth and improve the material quality. Surfactant denotes a substance that modifies the growth morphology, in our case promoting 2D growth, either by decreasing the surface free energy or by altering the surface kinetics.[59] Furthermore, the surfactant segregates at the growth front, without being incorporated. Concerning GaN MBE growth, the addition of As,[60,61] H,[62] or In (Refs. 63–65) has been reported to favor 2D growth under slightly N-rich conditions.

In this work, we describe the optimization of the growth of GaN/AlN superlattices, which implies determining the adequate III/V ratio to attain droplet-free 2D layers and the substrate temperature range that is compatible for both GaN and AlN growth. Three approaches have been considered: use of In as a surfactant (IS), use of a Ga excess (GS), and use of a Ga excess for GaN and an Al excess for AlN, this latter approach requiring growth interruptions (GI).

1. Use of In as a surfactant

Indium has been reported to behave as a surfactant for III-nitride PAMBE growth, since it favors 2D growth under slightly N-rich conditions.[63–65] From a theoretical point of view, indium is a particularly suitable choice, since a 1×1 In adlayer reduces the GaN(0001) surface energy[66] and decreases the diffusion barrier of nitrogen adatoms.[53] In a previous work, we have demonstrated the capability of In as a surfactant for AlGaN growth, delimiting the range of substrate temperatures and In fluxes at which an In adlayer is dynamically stable on $Al_xGa_{1-x}N(0001)$.[65] The efficiency of In as a surfactant for the growth of GaN/AlGaN MQW structures with low Al mole fraction ($\leq$25%) has also been proven.[67] However, the feasibility of this growth procedure for AlN growth has not been demonstrated.

In the present work, we have applied this growth procedure to GaN/AlN MQW structures. In this case, the Ga and Al fluxes are fixed to their stoichiometric value and an additional In flux is provided during the whole growth process to guarantee 2D growth. It is necessary to reduce the growth temperature to a value low enough to guarantee that In wets the growing surface, but remaining at a temperature high enough to prevent In incorporation [i.e., $T_S > 650$ Å (Ref. 68)]. Therefore, we have fixed the growth temperature at 680 °C and we have adjusted the In flux to obtain an In coverage of 1 ML during growth.

2. Use of a Ga excess

As discussed above, the 2D growth of GaN is optimized under slightly Ga-rich conditions, in a flux range characterized by the presence of a self-regulated Ga film, about 2 ML thick on the growth front. The stabilization of this Ga bilayer is possible for growth temperatures higher than 700 °C.

In the case of AlN, a possibility to achieve 2D growth consists of using Ga as a surfactant for the growth of AlN, with the Al flux corresponding to the Al/N stoichiometry and using an additional Ga flux to stabilize the surface. Since the Al–N binding energy is much higher than the Ga–N binding energy, Ga segregates on the surface and is not incorporated into the AlN layer.[69]

In the present work, we have assessed the growth of MQW structures using a 2 ML thick Ga-excess layer during both the growth of GaN and AlN (GS growth procedure). As this Ga excess is maintained during the growth of both QWs and barriers, no growth interruptions are required. The temperature of the substrate is fixed around 720 °C.

Figure 1 presents the evolution of the Ga coverage during growth as a function of the Ga flux, for a substrate temperature of 720 °C, together with AFM images illustrating the surface morphology of various GaN/AlN superlattices. We observe that the structural quality of GaN/AlN superlattices is particularly sensitive to the Ga/N ratio; the strain fluctuations induced by alternating GaN and AlN layers favor the formation of V-shaped pits, even in the Ga-bilayer growth window.[70,71]

Strain relaxation by V-pit formation at terminated dislocations is commonly observed in GaN-related materials, particularly in the InGaN/GaN system,[72] where the majority of threading dislocations has no driving force to glide or is kinetically impeded to glide at the growth temperature. V pits are generally inverted hexagonal pyramids with {10—11} facets. The nucleation of V pits depends on the energy balance between the decrease in elastic energy accumulated in the layer and the increase in surface energy due to the defect formation. The increase in surface energy is a function of the relative energies of the (0001) and {10—11} facets.[66] In the case of the GaN/AlN system, these defects are minimized by increasing the Ga flux, so that growth is performed at the limit of Ga accumulation on the surface, as shown in the AFM images of GaN/AlN superlattices (GaN in the last layer) in Fig. 1. This is explained by the strong decrease in the (0001) surface energy with increasing III/V ratio,[73] which favors 2D growth.

3. Use of a Ga excess for GaN and an Al excess for AlN with growth interruptions

Finally, we have studied the possibility to grow the AlN barriers under Al-rich conditions and the GaN QWs under Ga-rich conditions (GI growth procedure). It must be remembered that Al does not desorb from the surface at standard growth temperatures for GaN. Therefore, to prevent Al accumulation at the surface, it is necessary to perform periodic growth interruptions under nitrogen after the growth of the AlN barriers.

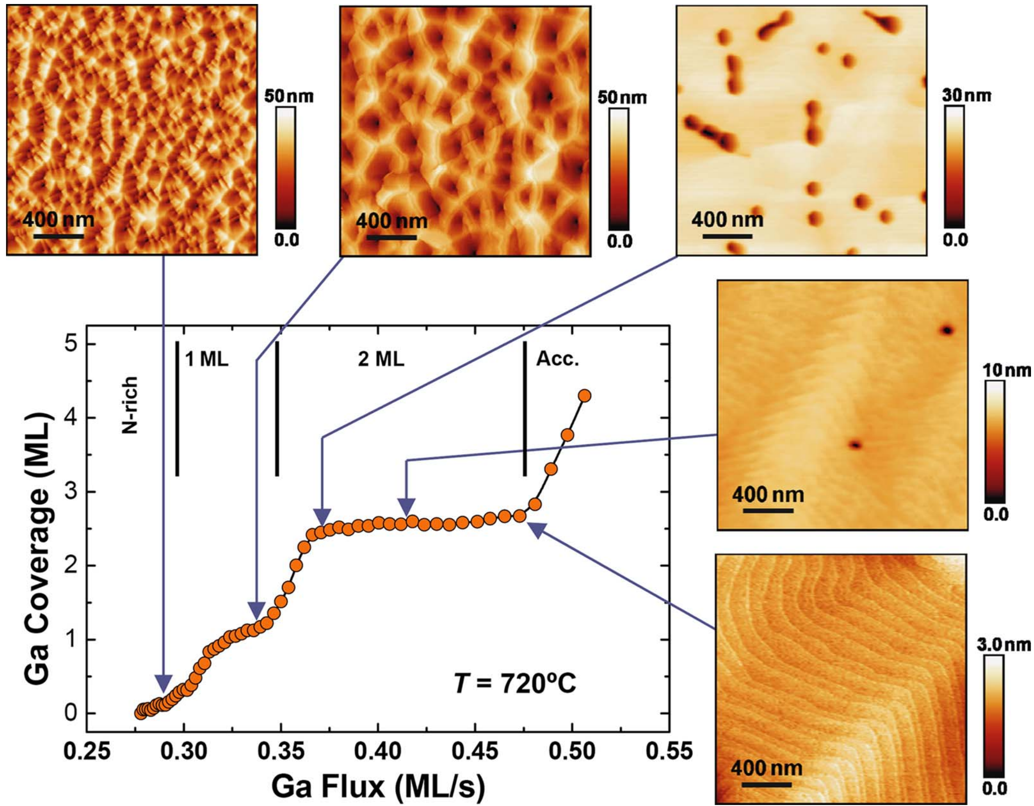

FIG. 1. (Color online) Variation in the surface morphology of GaN/AlN MQW structures as a function of the Ga coverage during growth.

4. Comparison of the various growth procedures

We have compared the structural quality of a series of samples grown using In as a surfactant, using Ga excess during the growth of the whole MQW structure, and using Ga excess for GaN and Al excess for AlN, this approach requiring growth interruptions. The samples considered for this study consist of 20 periods of Si-doped GaN QWs with a thickness in the range of 1–2 nm and 3-nm-thick AlN barriers. This active region is deposited on a 80-nm-thick GaN layer. The samples are capped with a 10-nm-thick GaN layer. The Si concentration is $\sim 5\times10^{19}$ cm^{-3} in the QWs and $\sim 7\times10^{17}$ cm^{-3} in the GaN layers. The growth method and the QW thickness measured by HRXRD are detailed in Table I.

The samples have been analyzed and compared in terms of surface morphology, GaN/AlN interface quality, and crystalline quality. The surface morphology of the samples has been analyzed by AFM, as illustrated in Fig. 2. All samples present the typical morphology of flat GaN layers, with atomic-step terraces, and spiral hillocks. No macroscopic cracks are observed in any of the samples. The root-mean-square (rms) surface roughness presented in Table I remains around 0.6 nm on a surface of 2.5×2.5 μm^2.

High-resolution transmission electron microscopy (HRTEM) images of the samples are presented in Fig. 3. From the analysis of these images we conclude that the GaN/AlN interfaces are abrupt at the monolayer scale in the three cases. Monolayer fluctuations of the well thickness can be observed, with separation being comparable to the atomic terrace width observed by AFM.

A comparison of the crystalline quality of the samples was performed by HRXRD characterization. Figure 4 pre-

TABLE I. Description of a series of samples grown by different methods (GS: Ga as a surfactant; IS: In as a surfactant; and GI: Ga and Al as surfactants with growth interruption after the AlN barriers): QW thickness measured by HRXRD, AFM rms surface roughness measured in a 2.5×2.5 μm^2, and intensity and FWHM of the ω-scan of the (0002) XRD of the superlattice and of the GaN buffer layer.

				X-ray diffraction			
				SL		GaN	
Sample	Growth procedure	QW thickness (nm)	Surface roughness (nm)	Intensity (counts/s)	FWHM (arc sec)	Intensity (counts/s)	FWHM (arc sec)
E609	GS	1.30 ± 0.25	0.53	645	158	1046	126
E610	GI	1.77 ± 0.25	0.60	447	190	1042	172
E617	IS	1.20 ± 0.25	0.65	133	623	816	284

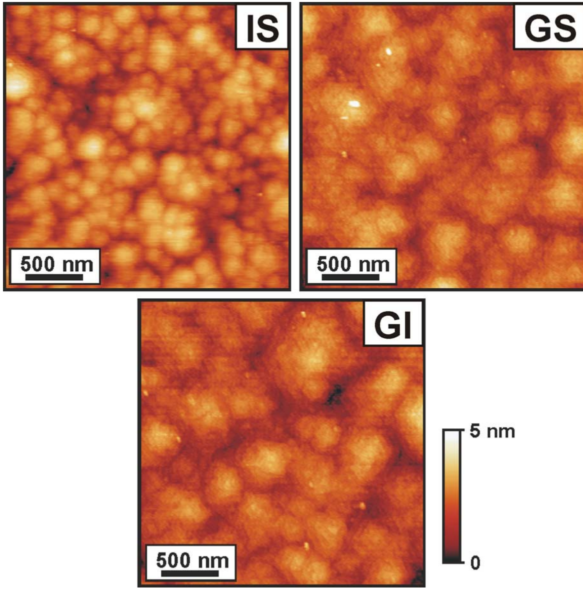

FIG. 2. (Color online) AFM images of samples grown by different methods: (a) E617 grown with In as a surfactant, (b) E609 grown with Ga excess, and (c) E610 grown using Ga and Al excess and with growth interruptions.

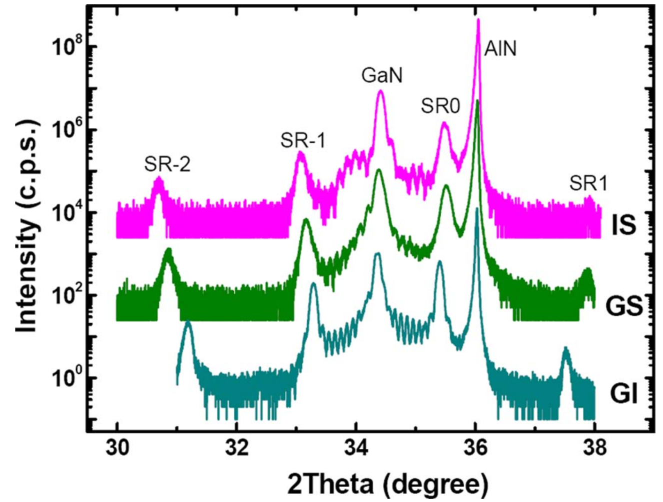

FIG. 4. (Color online) HRXRD θ-2θ scan of the (0002) reflection of GaN/AlN MQW structures grown using the IS, GS, and GI techniques, respectively.

sents the θ-2θ scans of the (0002) x-ray reflection of samples grown with In as a surfactant, using Ga excess and using both Ga excess and Al excess for the QWs and the barriers, respectively. In all cases, we observe several satellites of the superlattice reflection, which is an indication of the good quality of the interfaces. However, there are clear differences in the reflection intensity and the full width at half maximum (FWHM) of its (0002) ω-scan (both summarized in Table I), which can be correlated with the structural quality. Whereas the samples grown using the GS and GI procedures present comparable structural parameters, we observe that the sample grown with In as a surfactant presents a lower SL reflection intensity, and a significantly larger FWHM of the ω-scan. Let us remind that the FWHM of the ω-scan of the (0002) reflection is generally accepted as a first estimation of the structural quality of the samples, since the broadening is induced by screw and mixed dislocations. From the information in Table I, we hence conclude that the use of Ga excess (or the use of Ga excess for the QWs and Al excess for the barriers) results in superlattices with a better crystalline quality than in the case of using In as a surfactant.

In order to complete the comparison of these growth techniques, optical characterization by room-temperature cathodoluminescence (CL) was performed using an accelerating voltage of 5 keV, in order to maximize the signal emitted by the MQW region. Results presented in Fig. 5 show that in all cases the CL spectra are dominated by the band edge emission around 3.5–3.6 eV. However, the use of a Ga excess without growth interruptions makes it possible to minimize the emission from the defect band around 3.1 eV. Since no significant structural differences are found when comparing samples synthesized by the GS and GI methods,

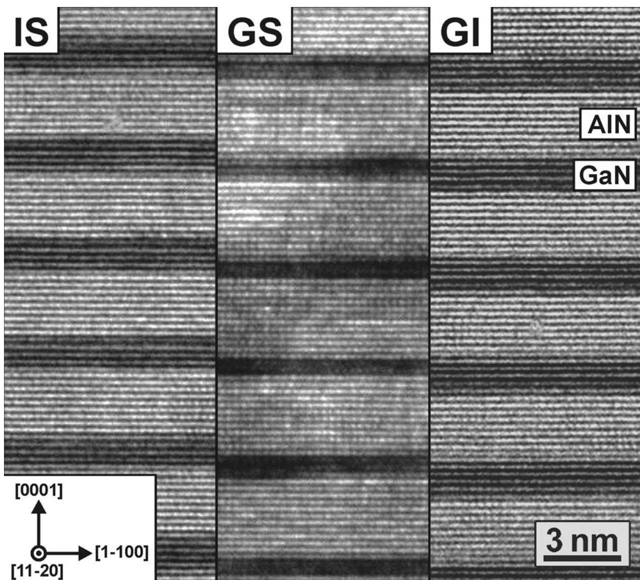

FIG. 3. HRTEM images of GaN/AlN MQW structures grown using the IS, GS, and GI techniques, respectively.

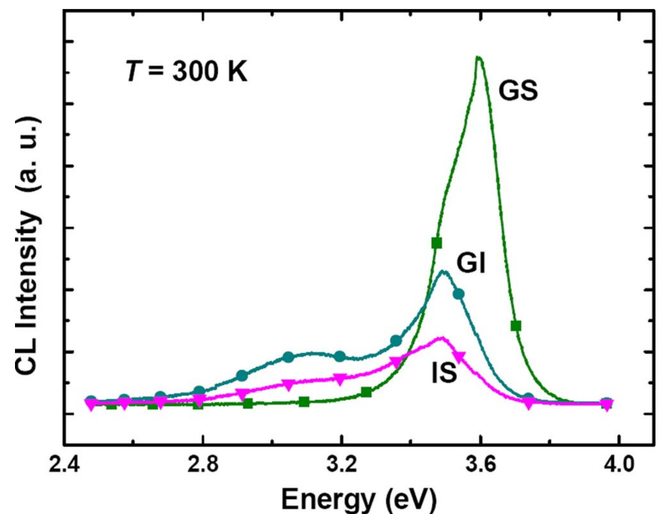

FIG. 5. (Color online) Room-temperature CL spectra from GaN/AlN MQW structures grown using the IS, GS, and GI techniques, respectively.

the difference in optical properties is attributed to possible contamination during the growth interruptions required by the GI procedure.

In summary, all samples present a good surface morphology and sharp GaN/AlN interfaces. Therefore, any of the growth procedures can be applied to the synthesis of short-period GaN/AlN superlattices. However, the results of XRD point out a lower crystalline quality in the case of growth using In as a surfactant, and optical characterization reveals a degradation of the performance when introducing growth interruptions. Therefore, for the studies presented in this paper, most of the samples were synthesized using Ga excess (GS growth mode). However, the use of Al excess and growth interruptions (GI growth mode) is necessary for samples with barriers thicker than 5 nm. For 5 nm nominal barriers deposited without growth interruptions (GS growth mode), an error of +5% in the growth rate calibration combined with an error of +5% in the Al flux calibration would result in a barrier thickness of 5.5 nm instead of 5 nm (i.e., 2 ML thicker than nominally expected) and therefore a reduction in the QW thickness by 2 ML. These error bars are reasonable, if we consider the calibration techniques and drifts of the Ga and N flux. By introducing a growth interruption after deposition of the AlN barrier, the thickness of the well becomes independent of the Al flux, and the uncertainty in the QW thickness is reduced to 1 ML.

5. Effect of Si doping

High *n*-type doping is required to populate the first electronic levels of the QWs and hence enable efficient ISB absorption. Silicon is a shallow donor, which can be easily incorporated in substitution of Ga in GaN layers. It can hence be considered as the impurity of choice for *n*-type doping of GaN. However, it has been reported that Si has an adverse effect on the surface morphology of GaN films. Small amounts of Si modify the GaN growth mode from a 2D step-flow growth to three dimensional growth, giving rise to the formation of islands, both in MOVPE (Ref. 74) and PAMBE.[75] It has also been suggested that Si induces roughness[76] and cracks,[77] and it might segregate at the surface.[78] This degradation of the layers has been attributed to the formation of Si_3N_4 precipitates when the layers are deposited under N-rich conditions.[79]

In our case, for thick GaN or $Al_xGa_{1-x}N$ ($x \leq 0.65$) layers grown by PAMBE under Ga-rich conditions, we do not observe any perturbation of the Ga kinetics during GaN growth in presence of Si.[80] Furthermore, no difference in the structural quality of GaN/AlN MQWs has been observed by AFM or HRXRD when comparing undoped and heavily doped structures ($[\mathrm{Si}] \sim 1 \times 10^{20}$ cm^{-3}). Discussion on the optical properties as a function of Si doping is presented below.

B. Electronic structure

It is well known that the optical properties of nitride QWs are strongly affected by the presence of an internal electric field.[81] This field, inherent to the wurtzite-phase nitride heterostructures grown along the [0001] axis, arises from the piezoelectric and spontaneous polarization discontinuity between the well and barrier materials. Modeling of quantum confinement in nitride QWs should therefore go beyond the flat-band approximation and account for the internal electric field in the QW and in the barriers. As an example, Fig. 6 presents the band diagram of GaN/AlN superlattices with different QW thicknesses (1 and 2 nm), calculated using the NEXTNANO3 8-band-$\mathbf{k} \cdot \mathbf{p}$ Schrödinger–Poisson solver.[82] The material parameters applied for the simulation are summarized in Table II. In a first approximation, the structures were considered strained on the AlN substrate. The potential takes on a characteristic sawtooth profile due to the internal electric field. The electron wave functions of the ground hole state h_1, the ground electron state e_1, and the excited electron states e_2 and e_3, are presented. Due to the built-in electric field, the electron wave functions are shifted toward the [0001] direction and the hole wave functions toward the [000–1] direction [quantum-confined Stark effect (QCSE)]. Regarding the conduction band structure, in narrow QWs ($\sim$1 nm) the energy difference between e_1 and e_2 is mostly determined by the confinement in the QW, whereas for larger QWs (>2 nm) this difference is mostly determined by the electric field, since both electronic levels lie in the triangular part of the QW potential profile. A de-

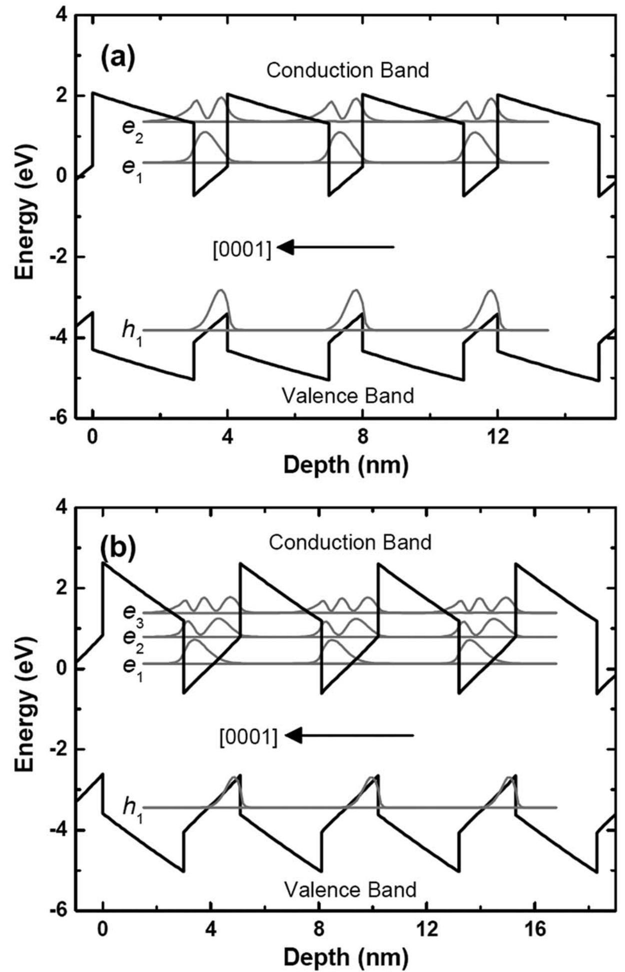

FIG. 6. Band diagram of GaN/AlN QWs in a superlattice with 3-nm-thick AlN barriers and (a) 4-ML-thick or (b) 8-ML-thick GaN QWs.

TABLE II. Material parameters used in the theoretical calculations. Data indicated with (*) were corrected to achieve a good fit with the experimental results.

Parameters	GaN	AlN	Refs.
Lattice constants (nm)			83
a	0.31892	0.3112	
c	0.51850	0.4982	
Spontaneous polarization [C m^{-2}]	−0.029	−0.081	81
Piezoelectric constants [C m^{-2}]			81
e_{13}	−0.49	−0.60	
e_{33}	0.73	1.46	
Elastic constants (GPa)			84 and 85
c_{11}	390	396	
c_{12}	145	137	
c_{13}	106	108	
c_{33}	398	373	
Dielectric constant	10	8.5	86
Luttinger parameters			87
A_1	−5.947	−3.991	
A_2	−0.528	−0.311	
A_3	5.414	3.671	
A_4	−2.512	−1.147	
A_5	−2.510	−1.329	
A_6	−3.202	−1.952	
A_7	0	0	
$E_P^{\parallel}$ (eV)	14(*)	17.3	
$E_P^{\perp}$ (eV)	14(*)	16.3	
Band offset (eV)	1.8		10

tailed description of the evolution of e_2-e_1 and e_3-e_1 with the QW thickness and strain state is presented below.

C. Optical characterization

The fundamental interband transition in MQW samples was probed by means of PL spectroscopy to assess the electric field in the wells. As described above, the e_1-h_1 transition is particularly sensitive to the electric field due to the QCSE. CL spectroscopy was used to get information on the in-plane homogeneity of the samples. Finally, the electronic structure was analyzed using FTIR spectroscopy.

1. Interband characterization

Figure 7 shows the low temperature (T=7 K) PL spectra of GaN/AlN MQW structures with 3-nm-thick AlN barriers and QW nominal thickness varying from 1.0 to 2.5 nm (4–10 ML). As expected, the PL peak energy is blueshifted by the quantum confinement in the thinner QWs (~1 nm) and strongly redshifted when increasing the QW thickness because of the QCSE. Assuming periodic boundary conditions, this internal electric field in the QWs F_W is proportional to the difference in polarization (spontaneous and piezoelectric) between the GaN in the QWs and the AlN in the barriers ΔP following the equation

$$F_W = \frac{\Delta P}{\varepsilon_0}\frac{l_B}{\varepsilon_B l_W + \varepsilon_W l_B}, \tag{1}$$

where ε_B, ε_W, and ε_0 are the dielectric constants of the barriers and of the wells and the vacuum permittivity, and l_B and

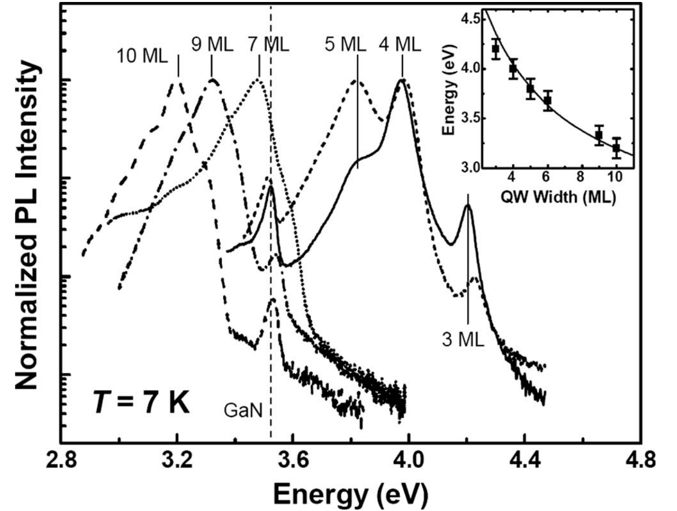

FIG. 7. Low-temperature (T=7 K) normalized PL spectra of GaN/AlN MQW structures with 3-nm-thick AlN barriers and different GaN QW thicknesses. In the inset, energy location of the low-temperature (T=7 K) PL peak as a function of the QW thickness. The solid line is a simulation assuming a polarization discontinuity $\Delta P/\varepsilon_0\varepsilon_r$=10 MV/cm.

l_W are the barrier and QW thickness, respectively. In the inset of Fig. 7, the PL peak energy from GaN/AlN MQWs with different thicknesses is compared to theoretical calculations of the e_1-h_1 transition assuming $\varepsilon_B=\varepsilon_W=\varepsilon_r$ and $\Delta P/\varepsilon_0\varepsilon_r$ =10 MV/cm.[10]

An important feature of the PL spectra is the presence of nonperiodical peaks or shoulders (see Fig. 7), which cannot be attributed to Fabry–Perot interferences. The energy locations of these different PL lines are summarized in Table III for the different superlattices. These PL peaks are located approximately at the same energies in the different samples, as indicated in Fig. 7. These discrete energy positions correspond to the expected values of the e_1-h_1 line in QWs whose thickness is equal to an integer number of GaN monolayers. For the very narrow QWs analyzed in this study, a variation in the thickness by 1 ML implies an important shift in the PL (about 150 meV for QWs of 4–5 ML). This value is larger than the FWHM of the PL lines, and hence results in well-resolved PL peaks instead of broadening the emission lines.

Thickness fluctuations can originate from a drift of the growth rate with time resulting in a variation in the QW thickness from well to well- or from in-plane inhomogeneities. In the samples under study, we have used a relatively low growth rate of 0.3 ML/s, and no drift of the growth rate was detected after 8 h of growth, as measured by reflection high-energy electron diffraction (RHEED) oscillations (error bar ~5%). Therefore, the thickness fluctuations from QW to QW should be significantly smaller than 1 ML. Regarding the in-plane homogeneity of the samples, we have performed low-temperature PL and CL studies in order to identify the possible origin of thickness fluctuations. Figure 8(a) presents the low-temperature PL spectrum from a 20-period GaN/AlN superlattice grown on a 500-nm-thick GaN buffer on an AlN-on-sapphire template (sample E935). It is important to outline that this sample contains cracks, due to the partially relaxed GaN buffer layer, which induces a tensile strain in the superlattice. The PL spectrum reproducibility when mea-

TABLE III. GaN/AlN MQW structures with an AlN barrier thickness of 3 nm and variable QW thickness. The value of QW thickness in the table corresponds to the nominal value except for the samples indicated by (1), which were measured by HRXRD or HRTEM. The PL measurements were performed at $T=7$ K, and the main PL peak is indicated in bold.

Sample	QW thickness (nm)	PLenergy (eV)	ISB Absorption (FWHM) (eV)	Absorption per reflection (%)
E580	1.25	⋯	0.883(0.083)	0.2
E589	1.25	⋯	0.881(0.159)	1.2
E601	1.0	3.48–**3.52**–4.02	0.927(0.099)	0.95
E603	1.0	⋯	0.932(0.101)	0.99
E607	$1.74 \pm 0.25(1)$	⋯	0.689(0.14)	2.2
E608	$1.51 \pm 0.25(1)$	**3.43**–3.51–3.61–3.76	0.729(0.134)	1.8
E609	$1.3 \pm 0.25(1)$	⋯	0.874(0.138)	3.4
E610	$1.77 \pm 0.25(1)$	**3.48**–3.58	0.7(0.123)	4.6
E611	$2.05 \pm 0.25(1)$	**3.41**–3.54	0.665(0.112)	4.1
E612	$2.20 \pm 0.25(1)$	**3.32**–3.54	0.649(0.08)	5.2
E617	$1.2 \pm 0.25(1)$	3.37–3.53–**3.64**–**3.69**–3.82	0.875(0.14)	1.2
E715	1.0	**3.82**–4.10	0.854(0.104)	0.6
E719	1.5	3.48–**3.57**–3.69–3.85	0.78(0.14)	3.6
E720	2.5	**3.20**–3.29–3.53	0.64(0.068)	4.7
E721	$2.13 \pm 0.25(1)$	⋯	0.685(0.105)	4.6
E756	$1.0 \pm 0.25(1)$	**3.82**–**3.98**–4.22	0.88(0.1)	1.5
E757	$0.75 \pm 0.25(1)$	3.82–**3.97**–4.20	0.895(0.095)	0.31
E777	$1.44 \pm 0.25(1)$	3.54–**3.64**	0.805(0.125)	1.5
E778	$1.72 \pm 0.25(1)$	**3.48**	0.745(0.140)	1.0
E779	$1.73 \pm 0.25(1)$	**3.47**	0.772(0.156)	0.54
E844	1.5	3.43–**3.52**–3.68	0.749(0.112)	2.9
E845	1.5	3.44–**3.52**–3.66	0.759(0.124)	3.6
E846	1.5	**3.42**–**3.52**–3.66	0.749(0.108)	3.6
E847	1.5	3.43–**3.53**–3.66	0.752(0.111)	3.6
E848	1.5	**3.42**–3.52–3.66	0.749(0.092)	2.7
E849	1.5	**3.42**–**3.52**–3.66	0.754(0.097)	4.0
E850	1.5	**3.47**	0.726(0.123)	4.1
E928	$0.9 \pm 0.1(1)$	**3.77**–3.94	0.868(0.056)	0.8
E930	$0.9 \pm 0.1(1)$	**3.79**–3.96	0.895(0.090)	1.0
E931	$0.9 \pm 0.1(1)$	**3.79**–3.96	0.911(0.089)	1.8
E933	$0.9 \pm 0.1(1)$	3.81–**3.79**	0.912(0.084)	1.6
E934	$0.9 \pm 0.1(1)$	**3.80**–3.96	0.906(0.081)	2.0
E935	$1.0 \pm 0.1(1)$	3.64–**3.77**–3.94	0.866(0.037)	0.03
E1041	1.0	3.86–**4.00**–4.22	0.904(0.155)	7.6
E1042	1.0	3.86–**3.99**–4.20	0.893(0.172)	5.8
E1043	1.0	3.86–**4.00**–4.22	0.905(0.128)	1.0
E1045	1.0	**4.02**–4.24	0.898(0.199)	2.5
E1047	1.0	**4.03**–4.23	0.875(0.217)	3.4

suring at different points of the sample (spot size ~200 μm, measured points separated by some millimeters) indicates a good long-range homogeneity. The PL spectrum presents three clearly identified lines at 3.95, 3.78, and 3.68 eV, in addition to the peaks corresponding to the band edge and the donor-acceptor recombination from the GaN buffer layer. If we compare the energy location of the PL lines with the results in Fig. 7, the peaks located at 3.95, 3.78, and 3.68 eV correspond to recombination in QWs with a thickness of 4, 5, and 6 ML, respectively. The three lines follow the expected evolution of the GaN band gap with temperature (not shown), which is consistent with its attribution to QW thickness fluctuations.

Figures 8(b)–8(d) present a low-temperature ($T=7$ K) CL map of E935, where we have selected the emission around the different PL lines presented in Fig. 8(a), i.e., around (b) 3.95, (c) 3.68, and (d) 3.78 eV. The energy window was ~150 meV and the acceleration voltage was chosen at 10 kV, so as to maximize the luminescence from the superlattice. Clearer regions correspond to higher CL intensity. We observe that the different emission lines originate from different regions of the sample. The luminescence at 3.68 eV is emitted from spots whose density is of the order of the dislocation density, as measured by TEM. The emission at 3.78 eV corresponds to the average active region of the sample. Finally, the luminescence at 4.00 eV is located at cracks in the structures. These cracks, due to the lattice mismatch between the GaN buffer layer and the superlattice, can be prevented by using an AlGaN buffer layer or strain engineering techniques that delay the relaxation of the GaN buffer—for instance, introducing periodic AlN barriers in the buffer layer to keep a compressive strain.

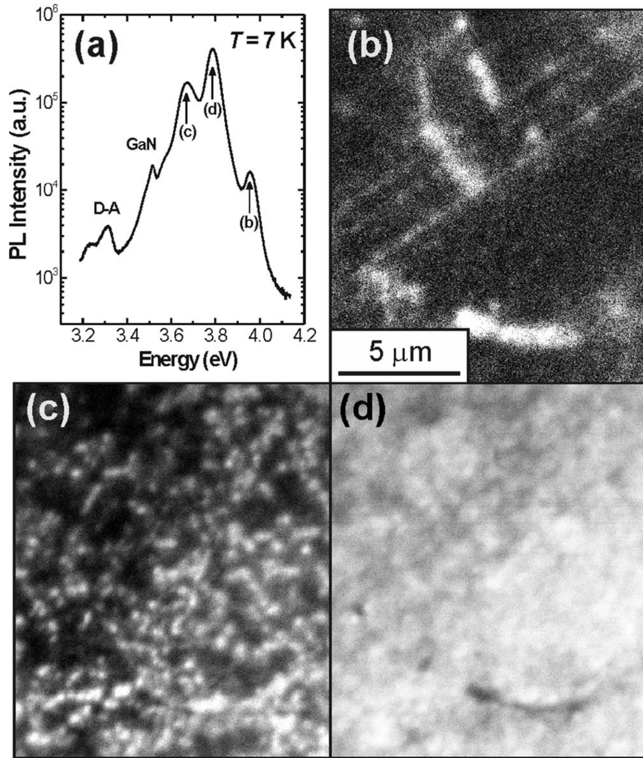

FIG. 8. Low-temperature (T=7 K) luminescence from a GaN/AlN MQW structure (sample E935): (a) PL spectrum and CL map around (b) 4.00 eV, (c) 3.68 eV, and (d) 3.78 eV. The energy window was ~150 meV, and the acceleration voltage was 10 keV for all the measurements. Clearer regions correspond to higher CL intensity.

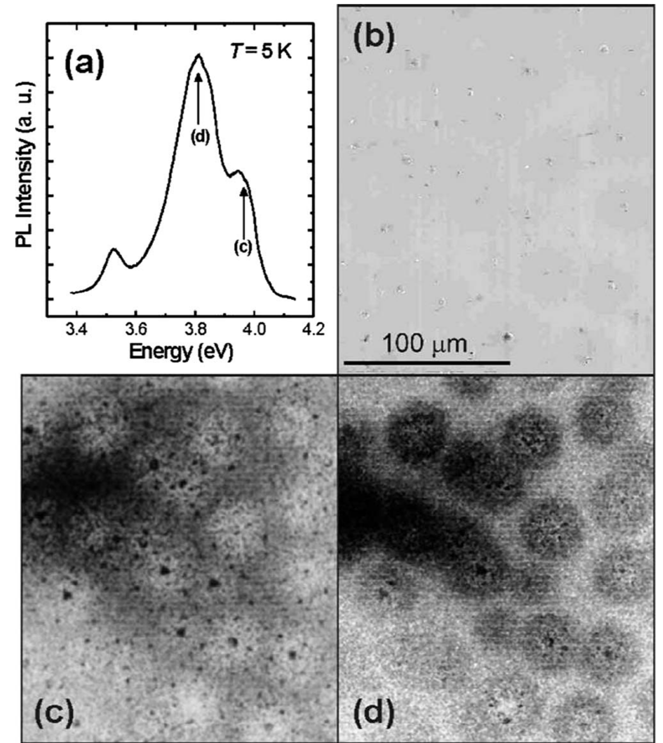

FIG. 9. Low-temperature (T=7 K) CL map of a GaN/AlN MQW structure (sample E1042) grown under Ga accumulation conditions: (a) CL spectrum, (b) surface morphology image in the scanning electron microscope, and CL map around (c) 3.82, and (d) 3.97 eV. The energy window was ~150 meV, and the acceleration voltage was 10 keV for all the measurements. Clearer regions correspond to higher CL intensity.

An additional source of thickness fluctuations occurs when growing under Ga accumulation conditions. The formation of droplets results in a local modification of the growth rate under the droplets, with the subsequent inhomogeneities in the QW luminescence. Figure 9(a) presents the low-temperature CL spectrum of a superlattice grown under Ga accumulation conditions. Two emissions at 3.97 and 3.82 eV are clearly identified, in addition to the luminescence from recombination in the GaN buffer layer. Although the metal droplets on the surface were removed by HCl etching, traces of the droplets are still visible as shadows in the surface image in Fig. 9(b). The CL maps presented in Figs. 9(c) and 9(d) were recorded at energies around 3.97 and 3.82 eV, respectively. The accelerating voltage was 10 keV, to maximize the signal coming from the QWs. The two luminescence lines are emitted in complementary regions of the sample, whose distribution corresponds to the Ga droplet distribution. The higher energy line is emitted by the material placed below the droplets, which points out a decrease in the growth rate in this area.

2. ISB absorption

The ISB absorption of a series of 20-period Si-doped AlN/GaN MQW structures with ~3 nm AlN barriers and different GaN QW thicknesses was investigated using FTIR.[10] As an example, Fig. 10 shows the ISB absorption of Si-doped AlN/GaN MQWs with QW thickness of 5, 6, 7, and 9 ML. The samples show a pronounced TM-polarized absorption, attributed to the transition from the first to the second electronic levels in the QW ($e_1 \rightarrow e_2$), while no absorption was observed for TE-polarized light within experimental sensitivity. The spectra present a Lorentzian-like shape, indicative of a homogeneously broadened absorption. The line width of the absorption remains in the 70–120 meV range for QWs doped at 5×10^{19} cm^{-2}, and the ISB absorption effi-

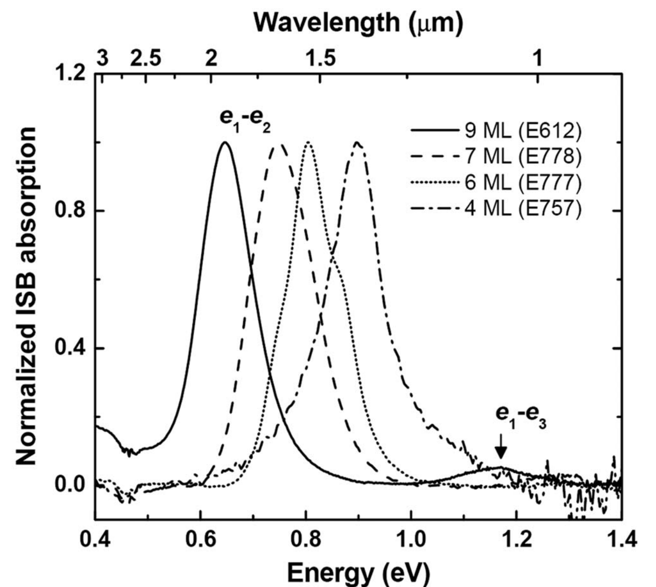

FIG. 10. Room-temperature TM-polarized ISB absorption spectra from Si-doped GaN/AlN MQW structures with 3-nm-thick AlN barriers and different GaN QW thicknesses.

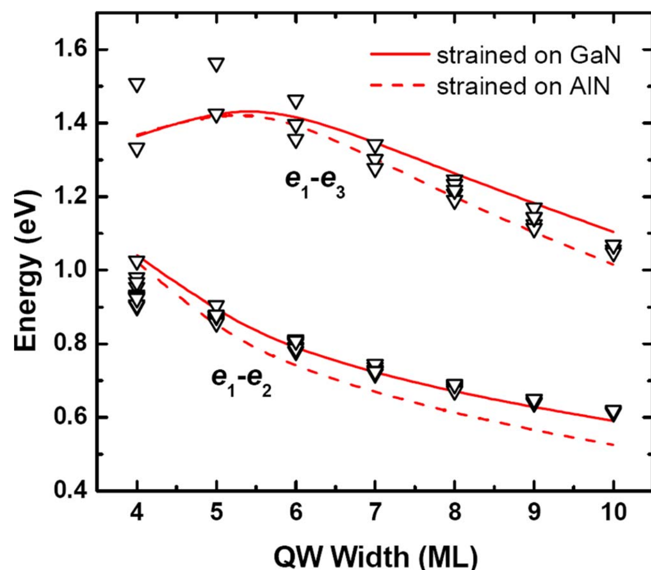

FIG. 11. (Color online) Variation in the e_1-e_2 and e_1-e_3 ISB transition energy as a function of the QW thickness in GaN/AlN superlattices with 3 nm thick AlN barriers. Triangles indicate experimental data and solid and dashed lines correspond to theoretical calculations assuming the structure fully strained on AlN and on GaN, respectively.

ciency per reflection attains 3%–5%. A record small line width of ~40 meV has been achieved in nonintentionally doped structures. The ISB absorption peak energy and the FWHM of a number of samples with 2–3 nm thick AlN barriers and variable QW thickness are summarized in Table III. The ISB absorption maximum can be tuned in the 1.33 to 1.91 μm wavelength range by changing the QW thickness from 4 to 10 ML. For large QWs (>8 ML), the $e_1 \rightarrow e_3$ transition is observed, as indicated in Fig. 10. This transition is allowed in nitride QWs because of the internal electric field in the well that breaks the symmetry of the potential. As observed in the PL measurements, the ISB absorption spectra present in general a multipeak structure, which can be attributed to monolayer thickness fluctuations.[10]

Figure 11 presents the experimental values of the e_1-e_2 and e_1-e_3 transitions as a function of the QW width for structures with 3 nm thick AlN barriers. The results are well fitted with theoretical calculations (solid and dashed lines in Fig. 11, assuming the structure fully strained on GaN and on AlN, respectively) using the NEXTNANO3 8-band-$\mathbf{k}\cdot\mathbf{p}$ Schrödinger–Poisson solver with the material parameters in Table II. The relevance of the strain stems from the higher piezoelectric coefficients of AlN compared to GaN, which results in an enhancement of the piezoelectric polarization, and hence of the internal electric field in the QW when the AlN barriers are tensile strained.

3. Photovoltaic measurements

To test the photovoltaic response, the above-described samples were first polished in a standard multipass geometry with a mirrorlike backside and two parallel 45° wedges. Planar photodetector devices are then fabricated by evaporation of two Ti/Au contacts on the sample surface. Optical response spectra are obtained by illumination of one of the contacts through a single 45° facet, while the other contact is

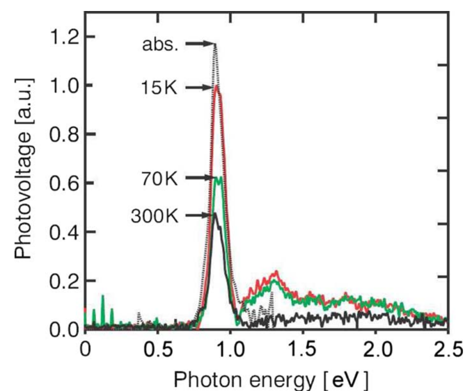

FIG. 12. (Color online) Photovoltaic response of GaN/AlN MQW structures measured as a function of temperature.

kept in the dark. The resulting photovoltage is amplified and fed into the external detector port of a FTIR spectrometer. As illustrated in Fig. 12, these devices display a spectrally narrow photovoltaic response to TM-polarized light around 1.55 μm at room temperature and can be operated at frequencies up to 2.94 GHz.[30,32]

The photovoltaic response of these structures has been explained as due to optical rectification.[31] The strong piezo and pyroelectric effects in this material family lead to intrinsic asymmetries of the electronic potential in the QWs, as illustrated in Fig. 6. Since in a GaN/AlN superlattice, the transition of an electron to an excited energy level implies a small displacement of the wave function in the growth direction, which results in the formation of an electrical dipole moment. For high electron density and in a multiple QW structure, these dipole moments add up and can be detected as an external photovoltage.

D. Strain in the superlattice: Influence of the substrate

As shown in Fig. 11, the simulations predict that the ISB transition energy in GaN/AlN MQWs depends on the strain state of the active region. Indeed, the higher piezoelectric constants of AlN compared to GaN result in an increase in the difference in piezoelectric polarization at the GaN/AlN interfaces when increasing the average *a* lattice constant of the superlattice. The subsequent enhancement of the internal electric field in the QWs should manifest in a blueshift in the e_1-e_2 energy difference. On the other hand, strain can also induce structural modifications during growth, favoring interdiffusion or degrading the QW interfaces, as experimentally demonstrated in Ref. 88.

In order to assess the role of the $Al_xGa_{1-x}N$ substrate and underlayers on the QW properties, we have *simultaneously* synthesized a series of GaN/AlN MQWs on different substrates: 4-μm-thick GaN-on-sapphire, 1-μm-thick $Al_{0.35}Ga_{0.65}N$-on-sapphire, 1-μm-thick $Al_{0.65}Ga_{0.35}N$-on-sapphire, and 1-μm-thick AlN-on-sapphire templates. The surface morphology of the substrates is presented in Figs. 13(a)–13(d). In the AFM images we can observe an enhancement of the surface roughness in the ternary substrates when compared with binary compounds. Nevertheless, all the substrates present atomic terraces, indicating a

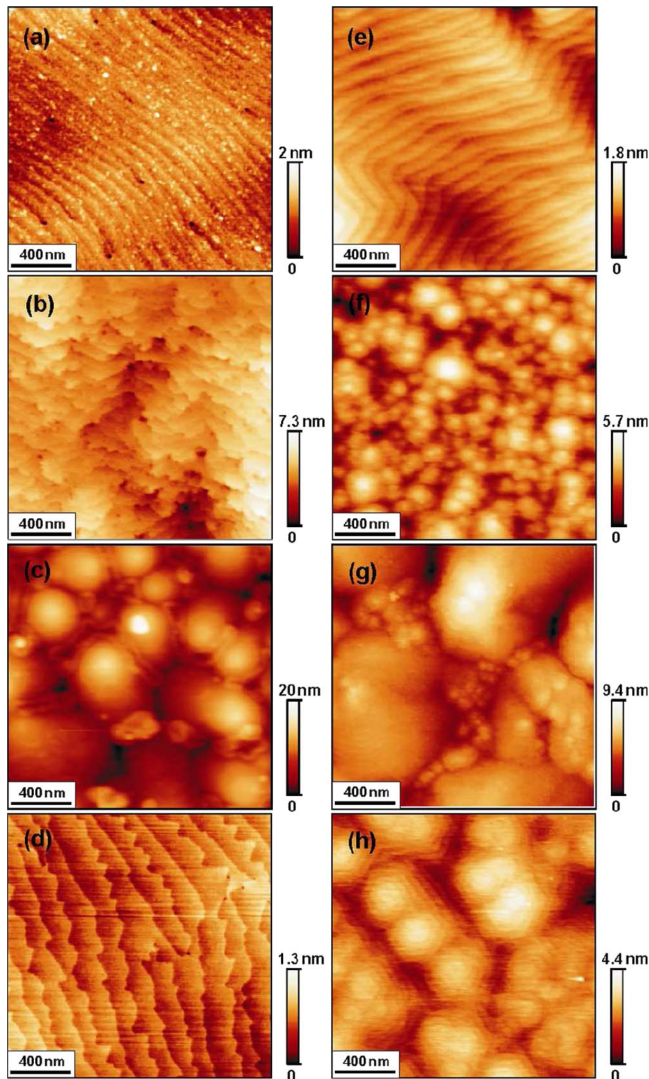

FIG. 13. (Color online) AFM surface analysis of (a) GaN-on-sapphire, (b) $Al_{0.35}Ga_{0.75}N$-on-sapphire, (c) $Al_{0.65}Ga_{0.35}N$-on-sapphire, and (d) AlN-on-sapphire templates, and of 20-period GaN/AlN (1.5/3 nm) MQW structures grown on (e) GaN-on-sapphire, (f) $Al_{0.35}Ga_{0.75}N$-on-sapphire, (g) $Al_{0.65}Ga_{0.35}N$-on-sapphire, and (h) AlN-on-sapphire templates.

short-scale roughness at the atomic layer scale.

The superlattices (series E1505 summarized in Table IV) consist of 30 periods of Si-doped GaN/AlN (1.25 nm/3 nm) MQWs, i.e., e_1-e_2 energy around 0.8 eV. Figure 13 presents a comparison of the surface morphology measured by AFM of

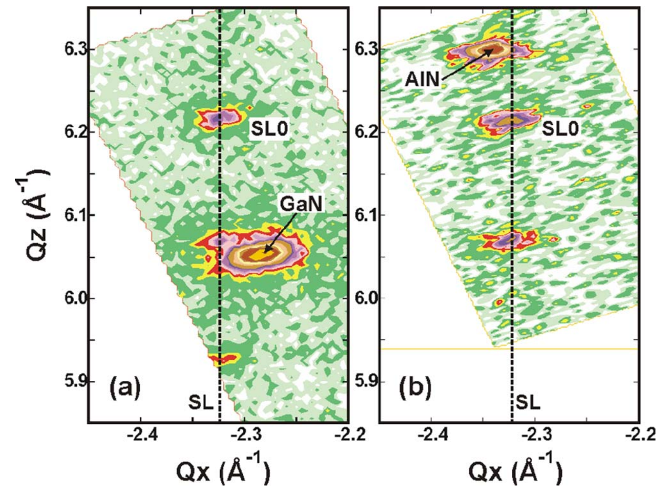

FIG. 14. (Color online) Reciprocal space map around the (10–15) x-ray reflection of GaN/AlN MQW structures grown (a) on GaN and (b) on AlN templates.

the samples deposited on (e) GaN, (f) $Al_{0.35}Ga_{0.65}N$, (g) $Al_{0.65}Ga_{0.35}N$, and (h) AlN templates. No cracks or macroscopic defects were observed in any of the samples. Best surface morphology is achieved by using binary compounds as a substrate, due to the better surface morphology of the respective templates. The rms surface roughness of samples grown on GaN or AlN is similar, but the hillock density, and hence the screw dislocation density, is higher in the case of AlN.

The average strain state of the superlattices was extracted from the ω-2θ scan of the (0002) x-ray reflection and the reciprocal space map of the (10—15) x-ray reflection, which is presented in Fig. 14 for the samples grown on GaN and AlN templates. For the four templates, the superlattices relax to an average lattice constant of $a=0.313\pm0.001$ nm, $c=0.5054\pm0.0005$ nm, i.e., an intermediate value between AlN and GaN, which is independent of the substrate. No variation in the superlattice period or composition was detected by XRD. The FWHM of the ω-scan of the (10—15) x-ray reflection is summarized in Table IV. This broadening, sensitive both to tilt and twist of the crystal, does not present significant differences from sample to sample, which indicates a comparable structural quality.

We have compared the lattice constants measured experimentally with the theoretical values expected in an infi-

TABLE IV. Series of GaN/AlN MQW structures grown on different $Al_xGa_{1-x}N$ templates: Al mole fraction of the substrate, FWHM of the ω-scan of the superlattice (10–15) x-ray reflection, PL peak energy and FWHM for the transition corresponding to 5 ML QW thickness, ISB absorption peak energy and FWHM, and magnitude of the ISB absorption per reflection. Note that the absorption spectrum consists of multiple peaks, and the ISB absorption FWHM values in this table correspond to the average value of a single peak.

Sample	Al content of the substrate	FWHM ω-scan (arc sec)	PL energy (eV)	ISB absorption (FWHM) (eV)	Absorption per reflection (%)
E1505A	100%	800	**3.556**–3.660	0.807(0.094)	8.5
E1505B	65%	795	**3.550**–3.656	0.805(0.080)	8.9
E1505C	35%	720	3.557–**3.664**	0.809(0.087)	8.1
E1505D	0%	810	3.574–**3.668**	0.809(0.087)	6.2

nite GaN/AlN superlattice without plastic relaxation. In superlattices with sufficiently thin AlN and/or GaN layers, the lattice constant mismatch is accommodated by elastic strain rather than by the formation of misfit dislocations. In this case, the elastic strain of the GaN and AlN layers can be calculated by considering the minimum of the elastic energy of the system. The elastic energy accumulated per unit of volume in a wurtzite semiconductor is given by

$$U = \tfrac{1}{2}c_{11}(\varepsilon_{11}^2 + \varepsilon_{22}^2) + \tfrac{1}{2}c_{33}\varepsilon_{33}^2 + 2c_{44}(\varepsilon_{13}^2 + \varepsilon_{23}^2) + (c_{11} - c_{12})\varepsilon_{12}^2 + c_{12}\varepsilon_{11}\varepsilon_{22} + c_{13}\varepsilon_{33}(\varepsilon_{11} + \varepsilon_{22}), \quad (2)$$

where c_{ij} and ε_{ij} are the elastic constants and the strain tensor elements, respectively. In the case of uniaxial strain—i.e., $\varepsilon_{11}=\varepsilon_{22}=(a\text{-}a_0)/a_0$; $\varepsilon_{33}=-2c_{13}\varepsilon_{11}/c_{33}$; $\varepsilon_{12}=\varepsilon_{13}=\varepsilon_{23}=0$; a_0 being the in-plane lattice parameter in bulk material— Eq. (2) is reduced to

$$U = \left(c_{11} + c_{12} - 2\frac{c_{13}^2}{c_{33}}\right)\varepsilon_{11}^2. \quad (3)$$

Therefore, in a period of an AlN/GaN superlattice, assuming no plastic deformation, the accumulated elastic energy per unit of surface is given by

$$U_S = l_B\left[\left(c_{11} + c_{12} - 2\frac{c_{13}^2}{c_{33}}\right)\varepsilon_{11}^2\right]_{\mathrm{AlN}} + l_W\left[\left(c_{11} + c_{12} - 2\frac{c_{13}^2}{c_{33}}\right)\varepsilon_{11}^2\right]_{\mathrm{GaN}}, \quad (4)$$

where l_B and l_W are the barrier and quantum well thickness, respectively. From this expression, we can determine the in-plane lattice parameter, which minimizes the elastic energy as

$$a = \frac{a_{\mathrm{AlN}}K_{\mathrm{AlN}} + a_{\mathrm{GaN}}K_{\mathrm{GaN}}}{K_{\mathrm{AlN}} + K_{\mathrm{GaN}}}, \quad (5)$$

where a_{AlN} and a_{GaN} are the in-plane lattice constants of bulk AlN and GaN, and K_{AlN} and K_{GaN} are given by

$$K_{\mathrm{AlN}} = \frac{l_B}{a_{\mathrm{AlN}}^2}\left(c_{11} + c_{12} - 2\frac{c_{13}^2}{c_{33}}\right)_{\mathrm{AlN}} \quad \text{and} \quad (6)$$

$$K_{\mathrm{GaN}} = \frac{l_W}{a_{\mathrm{GaN}}^2}\left(c_{11} + c_{12} - 2\frac{c_{13}^2}{c_{33}}\right)_{\mathrm{GaN}}.$$

In the case of the MQW structures under study, i.e., GaN/AlN (1.25/3 nm), and using the material parameters in Table II, the in-plane lattice parameter that minimizes the elastic energy in a period is $a=0.3140$ nm, beyond the error bars of the values measured by XRD. The difference between the experimental and calculated values is an indication of the presence of misfit dislocations in the superlattice. The difference in lattice parameter might be compensated by introduction of a misfit dislocation every ~50 nm in the AlN barrier. These results indicate a critical layer thickness smaller than the ~3 nm theoretically predictions by Bykhovski *et al.*[89]

The ISB optical properties of the samples grown on different substrates are summarized in Fig. 15 and Table IV. No significant change in the absorption peak energy location is observed for the different substrates. This result is consistent with the structural characterization by XRD and confirms that the lower growth temperature of PAMBE in comparison with MOVPE prevents the GaN/AlN interface degradation, which redshifts the ISB transition energies in MOVPE structures.[88] However, we observe a broadening of the overall spectrum for templates with higher Al content, probably due to the enhancement of thickness fluctuations in these substrates, which present a higher dislocation density.

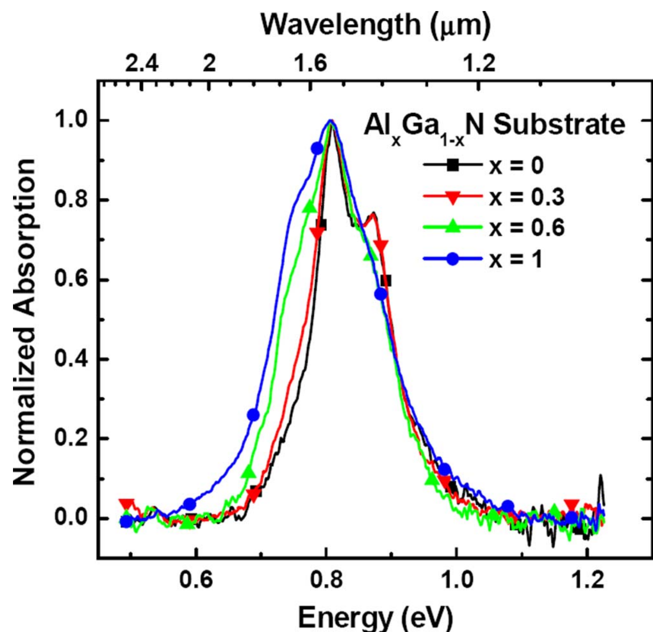

FIG. 15. (Color online) Room-temperature TM-polarized ISB absorption spectra from Si-doped GaN/AlN (1.5/1.5 nm) MQW structures grown on various $Al_xGa_{1-x}N$-on-sapphire templates.

E. Effect of the substrate temperature

In order to assess the effect of the growth temperature on the optical properties of the structures, we have synthesized a series of three samples grown at different substrate temperatures and consisting of 40 period GaN/AlN (1.5/1.5 nm) QWs grown on AlN-on-sapphire templates and capped with a 50-nm-thick AlN layer. The QWs were doped with a Si concentration of 5×10^{19} cm^{-3}. The substrate temperature is identified by RHEED measuring the Ga desorption time from GaN. Figure 16 displays the RHEED intensity transient due to Ga desorption after GaN growth in the regime of 2 ML of Ga excess at T_S=720, 725, and 730 °C, demonstrating the sensitivity of this method to resolve temperature changes in less than 5 °C.

The samples have been characterized by low-temperature PL as presented in Fig. 17(a). For increasing growth temperatures, we observe a decrease in the PL intensity together with a blueshift, which is explained by the QW thinning induced by AlN overgrowth.[90] The optical performance of low temperature samples in terms of PL correlates with the photovoltaic response of QWIPs fabricated on these samples. The low temperature (T=10 K) spectral response

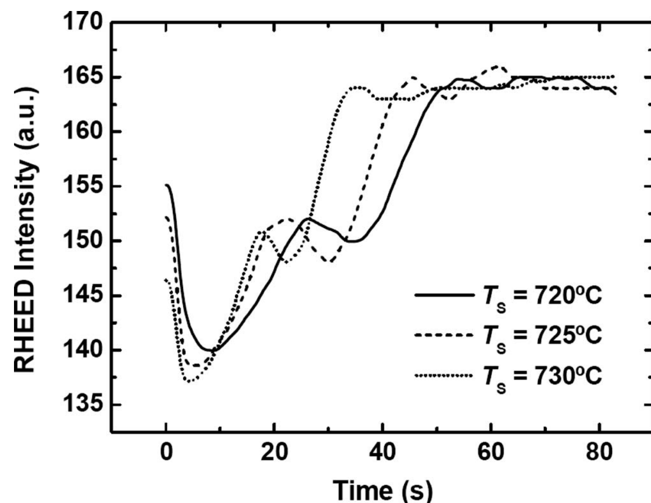

FIG. 16. RHEED intensity variation induced by Ga desorption from GaN at different substrate temperatures.

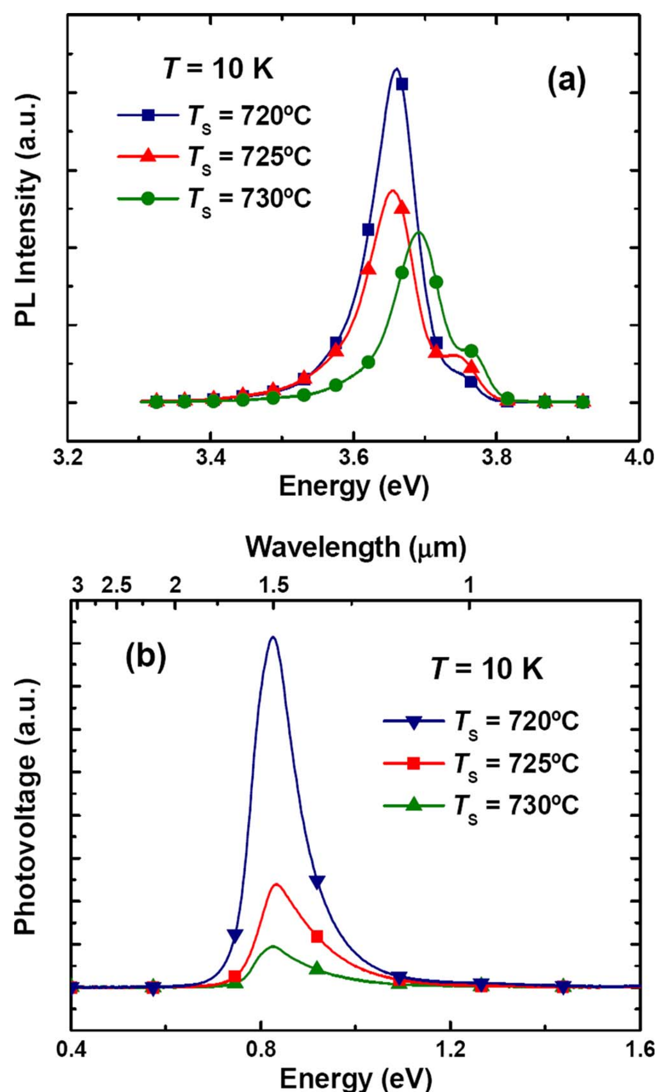

FIG. 17. (Color online) (a) Low-temperature (T=10 K) PL spectra from GaN/AlN MQW structures grown at different substrate temperatures. (b) Low-temperature (T=10 K) photovoltaic response of QWIPs fabricated on GaN/AlN MQW structures grown at different substrate temperatures.

displayed in Fig. 17(b) shows a decrease in the responsivity by almost one order of magnitude when increasing the growth temperature from 720 °C to 730 °C.

It is important to distinguish between the thermal-activated QW thinning process observed in PAMBE growth and the thermal- or strain-activated interdiffusion observed in MOVPE-grown structures.[88] In this latter case, the formation of an AlGaN layer at the interface results in a redshift in the ISB transition. In our case, there is no AlGaN intermixing; the GaN/AlN interface remains sharp but the QW is thinner, so that the absorption is slightly blueshifted.

F. Effect of Si doping

We have analyzed the effect of the Si-doping location in GaN/AlN MQW structures by growing samples with Si injected during the deposition of the QWs, during the deposition of the barriers, and also only in the middle of the QWs or in the middle of the barriers. In all the cases the doping level was $[\mathrm{Si}]=5\times10^{19}\ \mathrm{cm}^{-3}$. The samples under study consist of GaN/AlN (4 ML/3 nm) MQW structures grown on a 500-nm-thick GaN buffer layer on AlN-on-sapphire templates. The doping location and characterization data of these samples are summarized in Table V. From the structural point of view, we observed no significant difference in the top layer morphology characterized by AFM or in the FWHM of the ω-scan of the superlattice (0002) x-ray reflection, as shown in Table V. Furthermore, no significant difference in the strain state could be deduced from the $\omega-2\theta$ scan in the (0002) x-ray reflection. We hence conclude that Si does not alter the structural properties of the superlattices.

The PL peak energy and FWHM are compared in Table V. Si doped samples present a blueshift and broadening of the PL lines, as a result of band filling. The carrier screening of the internal electric field is negligible, according to the simulations of the electronic structure. Note that the observed blueshift is significantly smaller than the shift expected when increasing the QW thickness by 1 ML. Regarding ISB absorption, the absorption per reflection is in the range of 1% to 2% for all the doped samples, whereas the non-intentionally doped (n.i.d.) superlattices have a lower absorption value, which is consistent with a lower carrier density in these structures. The residual absorption is due to nonintentional doping of the QWs (estimated about $10^{17}\ \mathrm{cm}^{-3}$ from Hall measurements in GaN layers grown on AlN-on-sapphire templates) and of the AlN barriers, as well as to carrier transfer to the QWs induced by the internal electric field. Figure 18 displays the normalized TM-polarized ISB absorption for the samples under study. The absorption lines present a blueshift in the case of doped samples, which can be explained by many-body effects, dominated by exchange interactions.[7] Additionally, the line width increases from a record low value of 40–53 meV for n.i.d. samples to values of 80–90 meV for doped samples, whatever the Si location in the structure (see Table V).

We can hence conclude that the Si doping enhances, broadens, and blueshifts the ISB absorption of GaN/AlN

TABLE V. Series of GaN/AlN MQW structures with different Si doping locations: Si location, FWHM of the ω-scan of the superlattice (0002) x-ray reflection, PL peak energy and FWHM for the transition corresponding to 5 ML QW thickness, ISB absorption energy and FWHM, and magnitude of the ISB absorption per reflection. Note that the absorption spectrum consists of multiple peaks, and the ISB absorption FWHM values in this table correspond to the average value of a single peak.

Sample	Si position	FWHM ω-scan (arc sec)	PL energy (FWHM) (eV)	ISB absorption (FWHM) (eV)	Absorption per reflection (%)
E928	n.i.d.	360	3.77(0.053)	0.868(0.056)	0.8
E930	Wells	306	3.79(0.087)	0.895(0.090)	1.01
E931	Barriers	362	3.79(0.067)	0.911(0.089)	1.78
E933	Middle of the wells	312	3.81(0.094)	0.912(0.084)	1.63
E934	Middle of the barriers	326	3.80(0.082)	0.906(0.081)	1.99
E935	n.i.d.	420	3.77(0.040)	0.866(0.037)	0.03

multiple quantum well structures (Table V). However, no clearly identified effect could be related to the Si doping location.

G. Polarization-induced doping: Effect of the cap layer

In nitride heterostructures, the magnitude of the ISB absorption depends not only on the Si doping level in the QWs, but also on the presence of nonintentional dopants and on the carrier redistribution due to the internal electric field. In order to evaluate the contribution of the internal electric field induced by the cap layer to the ISB absorption, we have synthesized a series of 40-period nonintentionally doped GaN/AlN (1.5/1.5 nm) MQW structures where we varied the Al mole fraction of the 50-nm-thick $Al_xGa_{1-x}N$ cap layer. All the structures were grown on AlN-on-sapphire templates.

Measurements of ISB absorption in these samples, summarized in Fig. 19 and Table VI, confirm a monotonous increase and broadening of the absorption when increasing the Al mole fraction of the cap layer. These results are consistent with the simulations of the electronic structure in Fig. 20, where we observe that the use of AlN as a cap layer lowers the conduction band of the first GaN QWs below the Fermi level (dash-dotted line at 0 eV in the figures), whereas the use of GaN as a cap layer results in the depletion of the MQW active region. Therefore, we conclude that the internal electric field induced by the cap layer can result in a significant (even dominant) contribution to the infrared absorption in GaN/AlN MQW structures.

IV. CONCLUSIONS

In conclusion, we have studied the effect of PAMBE growth and design parameters on the performance of Si-doped GaN/AlN MQW structures for ISB optoelectronics in the near infrared. From the point of view of the growth procedure, best optical properties are obtained in samples synthesized with a moderate Ga excess during the growth of

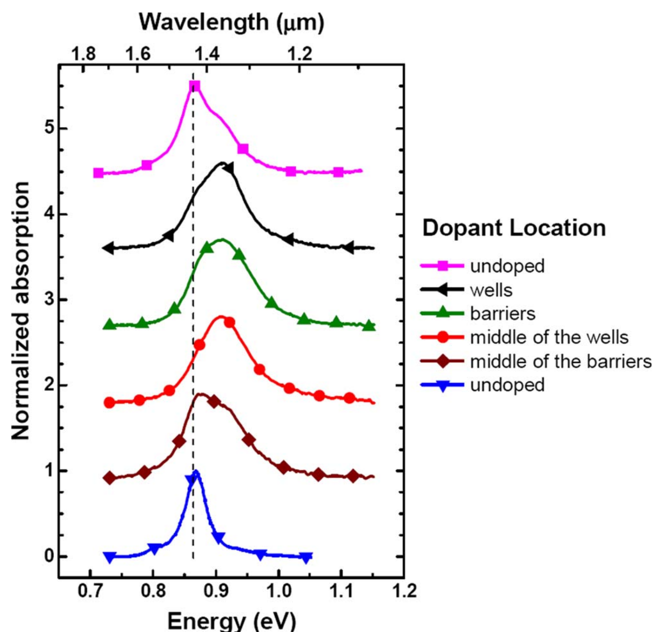

FIG. 18. (Color online) Room-temperature TM-polarized ISB absorption spectra of Si-doped GaN/AlN (1.5/3 nm) MQW structures grown doped in the QWs, in the barriers, in the middle of the wells, in the middle of the barriers, and undoped.

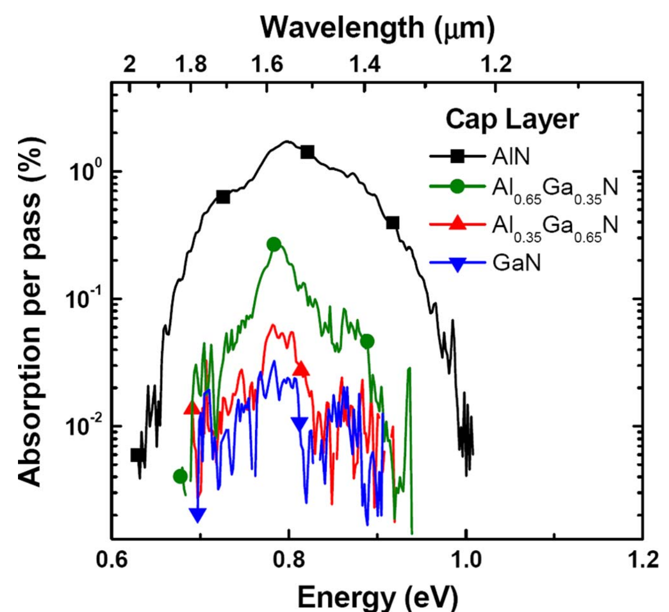

FIG. 19. (Color online) Room-temperature TM-polarized ISB absorption spectra of nonintentionally doped GaN/AlN (1.5/1.5 nm) MQW structures finished with a 50 nm thick $Al_xGa_{1-x}N$ cap layer with different Al mole fractions.

TABLE VI. Series of nonintentionally doped GaN/AlN (1.5/1.5 nm) MQW structures capped with 50 nm of $Al_xGa_{1-x}N$ with different Al mole fractions.

Sample	Al mole fraction in the cap layer	ISB absorption (FWHM) (eV)	Absorption per reflection (%)
E1487	100%	0.797(0.080)	1.7
E1488	65%	0.787(0.040)	0.26
E1489	35%	0.781 (–)	0.15
E1486	0%	–	<0.005

both the GaN QWs and the AlN barriers, without growth interruptions. The structural quality of the samples is independent of Si doping up to 10^{20} cm^{-3}. The optical properties are degraded at high growth temperatures (>720 °C) due to the thermal activation of the AlN etching of GaN. From the point of view of strain, GaN/AlN MQWs evolve rapidly to an equilibrium average lattice parameter, which is independent of the substrate. As a result, we do not observe any significant effect of the underlayers on the optical performance of the MQW structure. The average lattice parameter is different from the expected value from elastic energy minimization, which points out the presence of periodic misfit dislocations in the structure. It is found that the internal electric field due to piezoelectric and spontaneous polarization can deplete or induce charge accumulation in the QWs, which are particularly sensitive to the Al mole fraction in the cap layer. This polarization-induced doping can result in a significant, and even dominant, contribution to the infrared absorption in GaN/AlN MQW structures. In Si-doped samples, the ISB absorption spectrum broadens and blueshifts with doping as a result of electron-electron interactions. This behavior is independent of the Si doping location in the structure, either in the QWs or in the barriers.

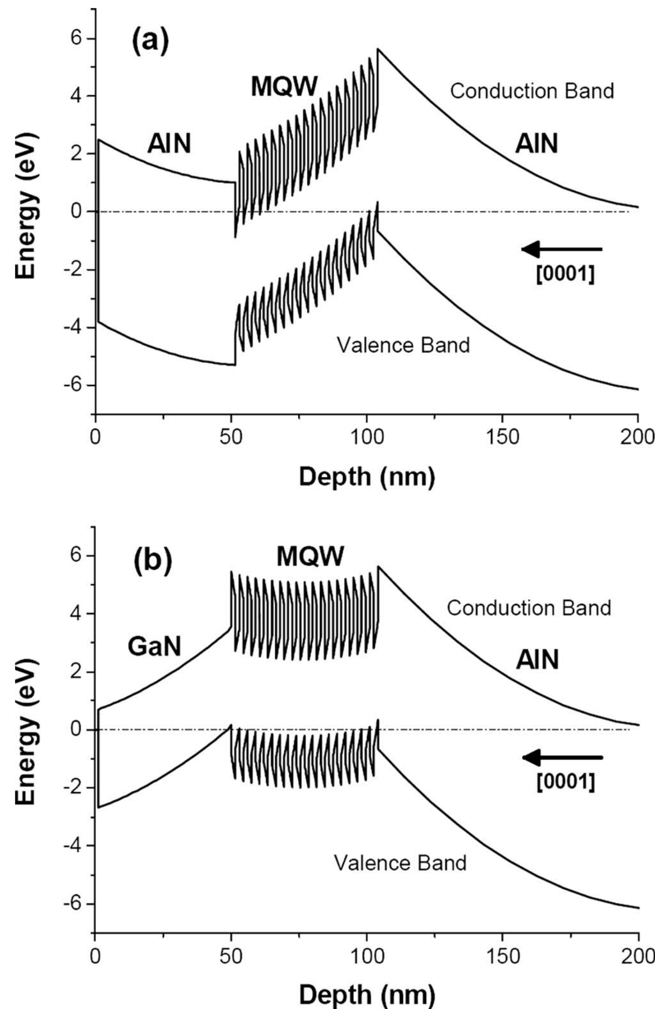

FIG. 20. Band diagram of nonintentionally doped GaN/AlN (1.5/1.5 nm) MQW structures with (a) AlN cap layer and (b) GaN cap layer.

ACKNOWLEDGMENTS

This work was partially supported by the 7th European Framework Program within DOTSENSE Project (FP7–IST-224212) and by ANR-06–BLAN-0130 TRANSNIT. Technical support from Y. Curé, J. Dussaud, Y. Genuist, and M. Terrier is acknowledged. AlN-on-sapphire templates were provided by DOWA Electronics Materials Inc.

[1]A. V. Gopal, H. Yoshida, A. Neogi, N. Georgiev, T. Mozume, T. Simoyama, O. Wada, and H. Ishikawa, IEEE J. Quantum Electron. **38**, 1515 (2002).
[2]R. Akimoto, B. S. Li, K. Akita, and T. Hasama, Appl. Phys. Lett. **87**, 181104 (2005).
[3]B. S. Ma, W. J. Fan, Y. X. Dang, W. K. Cheah, W. K. Loke, W. Liu, D. S. Li, S. F. Yoon, D. H. Zhang, H. Wang, and C. H. Tung, Appl. Phys. Lett. **91**, 051102 (2007).
[4]C. Gmachl, H. M. Ng, S. N. G. Chu, and A. Y. Cho, Appl. Phys. Lett. **77**, 3722 (2000).
[5]C. Gmachl, H. M. Ng, and A. Y. Cho, Appl. Phys. Lett. **79**, 1590 (2001).
[6]K. Kishino, A. Kikuchi, H. Kanazava, and T. Tachibana, Appl. Phys. Lett. **81**, 1234 (2002).
[7]A. Helman, M. Tchernycheva, A. Lusson, E. Warde, F. H. Julien, Kh. Moumanis, G. Fishman, E. Monroy, B. Daudin, L. S. Dang, E. Bellet-Amalric, and D. Jalabert, Appl. Phys. Lett. **83**, 5196 (2003).
[8]N. Suzuki and N. Iizuka, Jpn. J. Appl. Phys., Part 2 **38**, L363 (1999).
[9]S. Nicolay, J. F. Carlin, E. Feltin, R. Butte, M. Mosca, N. Grandjean, M. Ilegems, M. Tchernycheva, L. Nevou, and F. H. Julien, Appl. Phys. Lett. **87**, 111106 (2005).
[10]M. Tchernycheva, L. Nevou, L. Doyennette, F. H. Julien, E. Warde, F. Guillot, E. Monroy, E. Bellet-Amalric, T. Remmele, and M. Albrecht, Phys. Rev. B **73**, 125347 (2006).
[11]G. Cywiński, C. Skierbiszewski, A. Fedunieiwcz-Żmuda, M. Siekacz, L. Nevou, L. Doyennette, M. Tchernycheva, F. H. Julien, P. Prystawko, M. Kryśko, S. Grzanka, I. Grzegory, A. Presz, J. Z. Domagała, J. Smalc, M. Albrecht, T. Remmele, and S. Porowski, J. Vac. Sci. Technol. B **24**, 1505 (2006).
[12]G. Martin, S. Strite, A. Botchkarev, A. Agarwal, A. Rockett, W. R. L. Lambrecht, B. Segall, and H. Morkoç, J. Electron. Mater. **225**, 24 (1995).
[13]S. Wei and A. Zunger, Appl. Phys. Lett. **69**, 2719 (1996).
[14]G. Martin, A. Botchkarev, A. Rockett, and H. Morkoç, Appl. Phys. Lett. **68**, 2541 (1996).
[15]N. Iizuka, K. Kaneko, N. Suzuki, T. Asano, S. Noda, and O. Wada, Appl. Phys. Lett. **77**, 648 (2000).
[16]J. D. He, C. Gmachl, H. M. Ng, and A. Y. Cho, Appl. Phys. Lett. **81**, 1803 (2002).
[17]N. Iizuka, K. Kaneko, and N. Suzuki, Appl. Phys. Lett. **81**, 1803 (2002).
[18]J. Hamazaki, S. Matsui, H. Kunugita, K. Ema, H. Kanazawa, T. Tachibana, A. Kikuchi, and K. Kishino, Appl. Phys. Lett. **84**, 1102 (2004).
[19]N. Iizuka, K. Kaneko, and N. Suzuki, Opt. Express **13**, 3835 (2005).
[20]S. Valdueza-Felip, F. B. Naranjo, M. González-Herráez, H. Fernández, J. Solis, F. Guillot, E. Monroy, L. Nevou, M. Tchernycheva, and F. H. Julien, “,” IEEE Photonics Technol. Lett. **20**, 13662008.
[21]A. Rubio, J. L. Corkill, M. L. Cohen, E. L. Shirley, and S. G. Louie, Phys. Rev. B **48**, 11810 (1993).
[22]W. R. L. Lambrecht and B. Segall, in *Properties of Group III Nitrides*, EMIS Data Reviews Series No. 11, edited by J. H. Edgar (Inspec, London, 1994), Chap. 4.
[23]Y. Li, A. Bhattacharyya, C. Thomidis, T. D. Moustakas, and R. Paiella,

Opt. Express **15**, 5860 (2007).

[24]Kh. Moumanis, A. Helman, F. Fossard, M. Tchernycheva, A. Lusson, F. H. Julien, B. Damilano, N. Grandjean, and J. Massies, Appl. Phys. Lett. **82**, 868 (2003).

[25]M. Tchernycheva, L. Nevou, L. Doyennette, A. Helman, R. Colombelli, F. H. Julien, F. Guillot, E. Monroy, T. Shibata, and M. Tanaka, Appl. Phys. Lett. **87**, 101912 (2005).

[26]F. Guillot, E. Bellet-Amalric, E. Monroy, M. Tchernycheva, L. Nevou, L. Doyennette, F. H. Julien, L. S. Dang, T. Remmele, M. Albrecht, T. Shibata, and M. Tanaka, J. Appl. Phys. **100**, 044326 (2006).

[27]D. Hofstetter, S.-S. Schad, H. Wu, W. J. Schaff, and L. F. Eastman, Appl. Phys. Lett. **83**, 572 (2003).

[28]E. Baumann, F. R. Giorgetta, D. Hofstetter, H. Lu, X. Chen, W. J. Schaff, L. F. Eastman, S. Golka, W. Schrenk, and G. Strasser, Appl. Phys. Lett. **87**, 191102 (2005).

[29]D. Hofstetter, E. Baumann, F. R. Giorgetta, M. Graf, M. Maier, F. Guillot, E. Bellet-Amalric, and E. Monroy, Appl. Phys. Lett. **88**, 121112 (2006).

[30]F. R. Giorgetta, E. Baumann, F. Guillot, E. Monroy, and D. Hofstetter, Electron. Lett. **43**, 185 (2007).

[31]D. Hofstetter, E. Baumann, F. R. Giorgetta, F. Guillot, S. Leconte, and E. Monroy, Appl. Phys. Lett. **91**, 131115 (2007).

[32]D. Hofstetter, E. Baumann, F. Giorgetta, J. Dawlaty, P. George, F. Rana, F. Guillot, and E. Monroy, Appl. Phys. Lett. **92**, 231104 (2008).

[33]L. Doyennette, L. Nevou, M. Tchernycheva, A. Lupu, F. Guillot, E. Monroy, R. Colombelli, and F. H. Julien, Electron. Lett. **41**, 1077 (2005).

[34]A. Vardi, N. Akopian, G. Bahir, L. Doyennette, M. Tchernycheva, L. Nevou, F. H. Julien, F. Guillot, and E. Monroy, Appl. Phys. Lett. **88**, 143101 (2006).

[35]A. Vardi, G. Bahir, F. Guillot, C. Bougerol, E. Monroy, S. E. Schacham, M. Tchernycheva, and F. H. Julien, Appl. Phys. Lett. **92**, 011112 (2008).

[36]N. Iizuka, K. Kaneko, and N. Suzuki, Electron. Lett. **40**, 962 (2004).

[37]N. Iizuka, K. Kaneko, and N. Suzuki, J. Appl. Phys. **99**, 093107 (2006).

[38]Y. Li, A. Bhattacharyya, C. Thomidis, T. D. Moustakas, and R. Paiella, Opt. Express **15**, 17922 (2007).

[39]M. Tchernycheva, L. Nevou, L. Doyennette, F. H. Julien, F. Guillot, E. Monroy, T. Remmele, and M. Albrecht, Appl. Phys. Lett. **88**, 153113 (2006).

[40]K. Driscoll, A. Bhattacharyya, T. D. Moustakas, R. Paiella, L. Zhou, and D. J. Smith, Appl. Phys. Lett. **91**, 141104 (2007).

[41]E. Baumann, F. R. Giorgetta, D. Hofstetter, S. Leconte, F. Guillot, E. Bellet-Amalric, and E. Monroy, Appl. Phys. Lett. **89**, 101121 (2006).

[42]L. Nevou, N. Kheirodin, M. Tchernycheva, L. Meignien, P. Crozat, A. Lupu, E. Warde, F. H. Julien, G. Pozzovivo, S. Golka, G. Strasser, F. Guillot, E. Monroy, T. Remmele, and M. Albrecht, Appl. Phys. Lett. **90**, 223511 (2007).

[43]N. Kheirodin, L. Nevoum, H. Machhadani, P. Crozat, L. Vivien, M. Tchernycheva, A. Lupu, F. H. Julien, G. Pozzovivo, S. Golka, G. Strasser, F. Guillot, and E. Monroy, IEEE Photonics Technol. Lett. **20**, 724 (2008).

[44]L. Nevou, M. Tchernycheva, F. H. Julien, F. Guillot, and E. Monroy, Appl. Phys. Lett. **90**, 121106 (2007).

[45]L. Nevou, F. H. Julien, M. Tchernycheva, F. Guillot, E. Monroy, and E. Sarigiannidou, Appl. Phys. Lett. **92**, 161105 (2008).

[46]Y. Inoue,H. Nagasawa, N. Stone, K. Ishino, A. Ishida, H. Fujiyasu, J. J. Kim, H. Makino, T. Yao, S. Sakakibara, and M. Kuwabara, J. Cryst. Growth **256**, 65 (2004).

[47]V. D. Jovanovic, D. Indjin, Z. Ikonic, and P. Harrison, Appl. Phys. Lett. **84**, 2995 (2004).

[48]D. Indjin, Z. Ikonic, V. D. Jovanovic, N. Vukmirovic, P. Harrison, and R. W. Kelsall, Semicond. Sci. Technol. **20**, S237 (2005).

[49]A. Ishida, K. Matsue, Y. Inoue, H. Fujiyasu, H. J. Ko, A. Setiawan, J. J. Kim, H. Makino, and T. Yao, Jpn. J. Appl. Phys., Part 1 **44**, 5918 (2005).

[50]N. Vukmirovic, V. D. Jovanovic, D. Indjin, Z. Ikonic, P. Harrison, and V. Milanovic, J. Appl. Phys. **97**, 103106 (2005).

[51]G. Sun, J. B. Khurgin, and R. A. Soref, J. Appl. Phys. **99**, 033103 (2006).

[52]C. Adelmann, J. Brault, G. Mula, B. Daudin, L. Lymperakis, and J. Neugebauer, Phys. Rev. B **67**, 165419 (2003).

[53]J. Neugebauer, T. K. Zywietz, M. Scheffler, J. E. Northrup, H. Chen, and R. M. Feenstra, Phys. Rev. Lett. **90**, 056101 (2003).

[54]R. M. Feenstra, J. E. Northrup, and J. Neugebauer, MRS Internet J. Nitride Semicond. Res. **7**, 3 (2002).

[55]B. Heying, R. Averbeck, L. F. Chen, E. Haus, H. Riechert, and J. S. Speck, J. Appl. Phys. **88**, 1855 (2000).

[56]J. E. Northrup, J. Neugebauer, R. M. Feenstra, and A. R. Smith, Phys. Rev. B **61**, 9932 (2000).

[57]A. R. Smith, R. M. Feenstra, D. W. Greve, M. S. Shin, M. Skowronski, J. Neugebauer, and J. E. Northrup, J. Vac. Sci. Technol. B **16**, 2242 (1998).

[58]A. R. Smith, V. Ramachandran, R. M. Feenstra, D. W. Greve, A. Ptak, T. Myers, W. Sarney, L. Salamanca-Riba, M. Shin, and M. Skrowronski, MRS Internet J. Nitride Semicond. Res. **3**, 12 (1998).

[59]N. Grandjean and J. Massies, Phys. Rev. B **53**, R13231 (1996).

[60]G. Feuillet, H. Hamaguchi, K. Ohta, P. Hacke, H. Okumura, and S. Yoshida, Appl. Phys. Lett. **70**, 1025 (1997).

[61]Y. Okamoto, S. Hashigushi, Y. Okada, and M. Kawabe, Jpn. J. Appl. Phys., Part 2 **38**, L230 (1999).

[62]T. Zywietz, J. Neugebauer, M. Scheffler, J. Northrup, and C. G. Van de Walle, MRS Internet J. Nitride Semicond. Res. **3**, 26 (1998).

[63]F. Widmann, B. Daudin, G. Feuillet, N. Pelekanos, and J. L. Rouvière, Appl. Phys. Lett. **73**, 2642 (1998).

[64]C. Kruse, A. Einfeldt, T. Bottcher, and D. Hommel, Appl. Phys. Lett. **79**, 3425 (2001).

[65]E. Monroy, B. Daudin, E. Bellet-Amalric, N. Gogneau, D. Jalabert, F. Enjalbert, J. Brault, J. Barjon, and L. S. Dang, J. Appl. Phys. **93**, 1550 (2003).

[66]J. E. Northrup and J. Neugebauer, Phys. Rev. B **60**, R8473 (1999).

[67]E. Monroy, F. Guillot, B. Gayral, E. Bellet-Amalric, D. Jalabert, J.-M. Gérard, L. S. Dang, M. Tchernycheva, and F. H. Julien, J. Appl. Phys. **99**, 093513 (2006).

[68]E. Monroy, N. Gogneau, D. Jalabert, E. Bellet-Amalric, Y. Hori, F. Enjalbert, L. S. Dang, and B. Daudin, Appl. Phys. Lett. **82**, 2242 (2003).

[69]E. Iliopoulos and T. D. Moustakas, Appl. Phys. Lett. **81**, 295 (2002).

[70]T. Nakamura, S. Mochizuki, S. Terao, T. Sano, M. Iwaya, S. Kamiyama, H. Amano, and I. Akasaki, J. Cryst. Growth **237–239**, 1129 (2002).

[71]M. Hermann, E. Monroy, A. Helman, B. Baur, M. Albrecht, B. Daudin, O. Ambacher, M. Stutzmann, and M. Eickhoff, Phys. Status Solidi C **1**, 2210 (2004).

[72]T. L. Song, J. Appl. Phys. **98**, 084906 (2005).

[73]A. L. Rosa and J. Neugebauer, Phys. Rev. B **73**, 205346 (2006).

[74]X.-Q. Shen, S. Tanaka, S. Iwai, and Y. Aoyagi, Appl. Phys. Lett. **80**, 2008 (1998).

[75]S. Tanaka, M. Takeuchi, and Y. Aoyagi, Jpn. J. Appl. Phys., Part 2 **39**, L831 (2000).

[76]A. Cremades, L. Görgens, O. Ambacher, M. Stutzmann, and F. Scholz, Phys. Rev. B **61**, 2812 (2000).

[77]L. T. Romano, C. G. Van de Walle, J. W. Ager III, W. Götz, and R. S. Kern, J. Appl. Phys. **87**, 7745 (2000).

[78]A. Munkholm, C. Thompson, M. V. Ramana Murty, J. A. Eastman, O. Auciello, G. B. Stephenson, P. Fini, S. P. DenBaars, and J. S. Speck, Appl. Phys. Lett. **77**, 1626 (2000).

[79]A. L. Rosa, J. Neugebauer, J. E. Northrup, C.-D. Lee, and R. M. Feenstra, Appl. Phys. Lett. **80**, 2008 (2002).

[80]E. Monroy, T. Andreev, P. Holliger, E. Bellet-Amalric, T. Shibata, M. Tanaka, and B. Daudin, Appl. Phys. Lett. **84**, 2554 (2004).

[81]F. Bernardini, V. Fiorentini, and D. Vanderbilt, Phys. Rev. B **56**, R10024 (1997).

[82]NEXTNANO3 software, available on-line http://www.nextnano.de

[83]I. Vurgaftman and J. R. Meyer, J. Appl. Phys. **94**, 3675 (2003).

[84]A. Polian, M. Grimsditch, and I. Grzegory, J. Appl. Phys. **79**, 3343 (1996).

[85]A. F. Wright, J. Appl. Phys. **82**, 2833 (1997).

[86]S.-H. Park, Jpn. J. Appl. Phys., Part 1 **39**, 3478 (2000).

[87]P. Rinke, M. Winkelnkemper, A. Qteish, D. Bimberg, J. Neugebauer, and M. Scheffler, Phys. Rev. B **77**, 075202 (2008).

[88]S. Nicolay, E. Feltin, J.-F. Carlin, N. Grandjean, L. Nevou, F. H. Julien, M. Schmidbauer, T. Remmele, and M. Albrecht, Appl. Phys. Lett. **91**, 061927 (2007).

[89]A. D. Bykhovski, B. L. Gelmont, and M. S. Shur, J. Appl. Phys. **81**, 6332 (1997).

[90]N. Gogneau, G. Jalabert, E. Monroy, E. Sarigiannidou, J.-L. Rouvière, T. Shibata, M. Tanaka, J.-M. Gérard, and B. Daudin, J. Appl. Phys. **96**, 1104 (2004).